PROCEEDINGS OF THE ROYAL SOCIETY B

*Proc. R. Soc. B* (2005) **272**, 127–133
doi:10.1098/rspb.2004.2934
*Published online* 25 January 2005

# Morphogenesis of the branching reef coral *Madracis mirabilis*

**Jaap A. Kaandorp[1*], Peter M. A. Sloot[1], Roeland M. H. Merks[1†], Rolf P. M. Bak[2], Mark J. A. Vermeij[3] and Cornelia Maier[2]**

[1]*Section Computational Science, University of Amsterdam, Kruislaan 403, 1098 SJ Amsterdam, The Netherlands*
[2]*Netherlands Institute for Sea Research, PO Box 59, 1790 AB Den Burg, The Netherlands*
[3]*Cooperative Institute for Marine and Atmospheric Studies, NOAA Fisheries, Southeast Science Center, 75 Virginia Beach Drive, Miami, FL 33149, USA*

Understanding external deciding factors in growth and morphology of reef corals is essential to elucidate the role of corals in marine ecosystems, and to explain their susceptibility to pollution and global climate change. Here, we extend on a previously presented model for simulating the growth and form of a branching coral and we compare the simulated morphologies to three-dimensional (3D) images of the coral species *Madracis mirabilis*. Simulation experiments and isotope analyses of *M. mirabilis* skeletons indicate that external gradients of dissolved inorganic carbon (DIC) determine the morphogenesis of branching, phototrophic corals. In the simulations we use a first principle model of accretive growth based on local interactions between the polyps. The only species-specific information in the model is the average size of a polyp. From flow tank and simulation studies it is known that a relatively large stagnant and diffusion dominated region develops within a branching colony. We have used this information by assuming in our model that growth is entirely driven by a diffusion-limited process, where DIC supply represents the limiting factor. With such model constraints it is possible to generate morphologies that are virtually indistinguishable from the 3D images of the actual colonies.

**Keywords:** morphogenesis; scleractinian corals; diffusion-limited growth; morphological plasticity; computed tomography scanning; stable isotope analysis



## 1. INTRODUCTION

Scleractinian corals are well known for their high morphological plasticity related to environmental forcing in light (Muko *et al.* 2000) and hydrodynamic (Bruno & Edmunds 1998; Kaandorp 1999) gradients. This externally driven morphological plasticity makes scleractinian corals extremely suitable for studying patterns of morphogenesis, and allows distinguishing intrinsic genetic regulation from external environmental forcings. However, experimental work on growth, colony shape and regeneration of corals is greatly limited by the difficulties experienced in accessing relevant local physical environmental parameters, such as micro-flow patterns, thickness of boundary layers, absorption of food particles (Sebens *et al.* 1997; Anthony 1999) and dissolved material (Sorokin 1993; Lesser *et al.* 1994; Marubini & Thake 1999; Marubini *et al.* 2002). As a case study to model growth and shape of phototrophic corals, we used the symbiont-bearing (zooxanthellate) coral species *Madracis mirabilis* (figure 1*a*,*b*). For zooxanthellate corals, the relevant physical environment consists of a phototrophic component with local calcification related to local light and inorganic carbon concentrations (Lesser *et al.* 1994; Marubini & Thake 1999; Marubini *et al.* 2002), and a heterotrophic component with local calcification related to the uptake of nutrients from the environment. Nutrients affecting the heterotrophic component can be either dissolved material (phosphate and nitrate) (Sorokin 1993) or particulate material (Sebens *et al.* 1997; Anthony 1999). The relative contribution of the phototrophic and heterotrophic components to the calcification can be estimated from skeletal $\delta^{13}C$ and $\delta^{18}O$ values by applying a model of kinetic versus metabolic isotope fractionation (McConnaughey *et al.* 1997; Heikoop *et al.* 2000; Maier *et al.* 2003).

In flume studies it was found that densely packed branching colonies, similar to those of *M. mirabilis*, act as a solid body (Chamberlain & Graus 1977). In a previous study we have performed simulation studies using actual morphologies of *M. mirabilis* in a laminar flow regime and found that around the branching morphologies, relatively large diffusive boundary layers are formed, which act as stagnant regions (Kaandorp *et al.* 2003). Flow starts to circumvent the colony and stagnant—and hence diffusion dominated—regions, even for relatively high flow velocities of up to 20 cm $s^{-1}$ (Chamberlain & Graus 1977), develop within the colony. Subsequently, photosynthetic bicarbonate assimilation results in depletion and gradients of dissolved inorganic carbon (DIC) within these boundary layers.

In *M. mirabilis* we observe a gradual change from more compact high-flow morphologies (for example the colony shown in figure 1*a*) at shallow locations to more open thin-branching low-flow morphologies at deeper locations

* Author for correspondence (jaapk@science.uva.nl).
† Present address: Indiana University, Biocomplexity Institute, Department of Physics, Swain Hall West 025, 727 East Third Street, Bloomington, IN 474045-7105, USA.

*Received* 10 June 2004
*Accepted* 8 September 2004

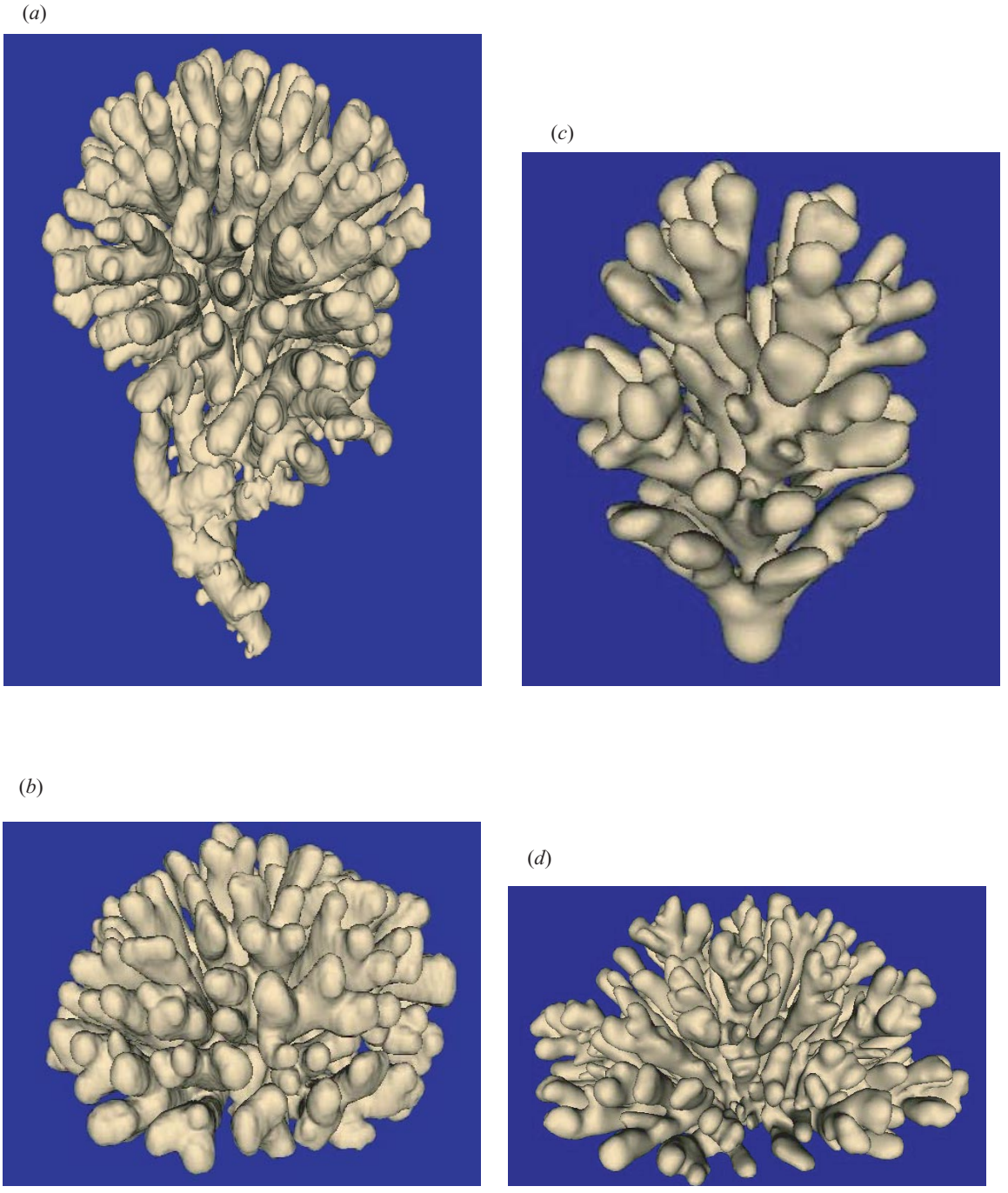


Figure 1. Surface-renderings of CT scans of *Madracis mirabilis* colonies and simulated objects. *C* indicates the compactness. (*a*) Upward-growing morphology ($C = 0.29$) and (*b*) hemispherical morphology ($C = 0.41$) of *M. mirabilis*. Simulated growth forms: (*c*) upward-growing morphology ($C = 0.30$) and (*d*) hemispherical morphology ($C = 0.24$). Animations of all objects shown in figure 1 can be found in electronic Appendix B.

(Kaandorp *et al.* 2003). In the branching coral *Pocillopora damicornis*, a similar morphological range is observed going from high-flow to low-flow locations (Veron & Pichon 1976). In Lesser *et al.* (1994) it was demonstrated that the morphological plasticity in *P. damicornis* provides a mechanism to minimize the diffusional boundary layer thickness and maximize mass transfer through the boundary layer under different flow regimes. In the compact high-flow morphology relatively smaller boundary layers develop, whereas in the open low-flow morphology, relatively larger boundary layers are formed. In both morphologies, under high-flow and low-flow conditions, respectively, sufficient transfer of nutrients through the boundary layer for the development of the colony is possible.

First, we have verified the assumption that calcification of *M. mirabilis* is mainly supported by photosynthesis through analysis of the $\delta^{13}C$ and $\delta^{18}O$ isotopes of the skeletons shown in figure 1*a*,*b* (Maier *et al.* 2003). If photosynthesis is the main source of energy then DIC gradients will play a crucial role in the morphogenesis of *M. mirabilis*. From growth models from physics (e.g. Brener *et al.* 1992) it is known that gradients of a growth-limiting agent may

induce branching patterns in abiotic growth processes. Our hypothesis is that gradients of a limiting nutrient (DIC) are required to induce a branching growth pattern in the development of coral colonies such as *M. mirabilis*. An alternative hypothesis is that the growth is mainly limited by local light intensities. Previous simulation studies (Graus & Macintyre 1982; Kaandorp & Kübler 2001) demonstrate that light-intensity-limited growth yields very different morphologies (for example spherical, column or plate-like morphologies), which may approximate the colony morphology of other coral species (for example, *Montastrea annularis*).

We have obtained actual morphologies of *M. mirabilis* (figure 1*a*,*b*) with computed tomography (CT) scanning techniques. This allows us to make a visual and quantitative comparison between the actual morphologies and the simulated growth forms. The goal is to construct a generative simulation model based on a minimal set of parameters and assumptions. With this model we want to simulate the full morphogenesis of the coral in space and time and compare the simulated results to actual three-dimensional (3D) morphological data. The purpose is to come to a 'minimal' model which has the highest explanatory and predictive power. We use a morphological simulation model, the accretive growth model, in combination with a diffusion model, to study the hypothesis that external gradients of inorganic carbon in the boundary layers of the colony are shaping the coral.

We have used a hydrodynamical model, based on the lattice Boltzmann method, that is suitable for computing flow patterns in complex-shaped 3D morphologies (Kaandorp *et al.* 2003). The method can be used in conjunction with a method to study the dispersion of a tracer through diffusion. Based on the findings in experimental work in flume studies (Chamberlain & Graus 1977) and previous simulation studies using actual *M. mirabilis* morphologies (Kaandorp *et al.* 2003), we have investigated the hypothesis that a diffusion-dominated model is sufficient to approximate the influence of external gradients of DIC on the growth process.

## 2. MATERIAL AND METHODS

### (a) *The computed tomography scans*

The *M. mirabilis* colonies were collected at depths between 6 m and 20 m at the reef of Curaçao (Netherlands Antilles, 12° N, 69° W). 3D images of the colonies were obtained using X-ray CT scanning techniques (Kaandorp & Kübler 2001). The CT scan data were stored in digital imaging and communications in medicine (DICOM) format (a general data format used for medical images). The CT scan data consist of $512 \times 512 \times z$ ($20 \leqslant z \leqslant 50$) 3D pixels, the so-called 'voxels'. The slice thickness of the CT scan data is 2.5 mm in the *xy* direction. Each voxel represents a density value between 0 and $2^{12}$, where 0 is the lowest density (the air around the coral skeleton), while high values indicate the calcium carbonate of the coral skeleton. In figure 1*a*,*b*, the 3D images are visualized using a surface rendering technique. The surface is constructed, approximately, at the boundary between the air and the calcium carbonate skeleton of the coral. With this technique, using the original dataset of $512 \times 512 \times z$ voxels, an image is reconstructed with an equal resolution in *x*, *y* and *z* directions (for details see Schroeder *et al.* 1997). Only the surface of the coral is visualized, without any surface structures such as corallites. On the voxels representing the surface of the corals a triangulated mesh was constructed using the marching cubes method (Lorensen & Cline 1987).

### (b) *Calculation of photosynthesis to respiration ratio*

We calculated the average photosynthesis to respiration (*P*/*R*) values using carbon ($\delta^{13}$C) and oxygen ($\delta^{18}$O) stable isotope data from carbonate samples (Maier *et al.* 2003) derived from the skeleton surface of the *M. mirabilis* colonies shown in figure 1*a*,*b* ($n = 36$ and $n = 78$, respectively), tissue $\delta^{13}$C samples (separated zooxanthellae and animal polyp, $n = 43$ each) of additional *M. mirabilis* colonies sampled between 5 m and 20 m depth, and $\delta^{18}$O and $\delta^{13}$C of sea water (seawater samples were taken in biweekly intervals between mid-April and the end of June 2001 at depths of 5 m, 15 m, 25 m and 40 m, $n = 36$). This dataset allowed us to calculate average *P*/*R* values for the *M. mirabilis* colonies based on the approaches described in McConnaughey *et al.* (1997) and Heikoop *et al.* (2000). We adjusted the equations for calculation of *P*/*R* values from stable isotope data as follows:

$$M_{\text{offset}} = \left(\delta^{13}C_{\text{orig}} - a\left(\delta^{18}O_{\text{orig}} - \delta^{18}O_{\text{eq}}\right) - \delta^{13}C_{\text{eq}}\right), \tag{2.1}$$

$$P/R = \frac{(M_{\text{offset}} - r)/r}{\delta^{13}C_z/\delta^{13}C_p}. \tag{2.2}$$

The parameters used in equations (2.1) and (2.2) are summarized in table 1.

There was no difference between depth effect on seawater $\delta^{13}$C or $\delta^{18}$O and consequently all data were put together and the average value was used to estimate the equilibrium values for aragonite in seawater. The samples of separated animal polyp and zooxanthellae tissues of *M. mirabilis* colonies for tissue $\delta^{13}$C analyses were retrieved from depths between 5 m and 20 m in June 2002 (C. Maier, unpublished data).

### (c) *Modelling diffusion*

We used a cellular-automata-based particle model, the 'moment propagation' method (Lowe & Frenkel 1995; Merks *et al.* 2002) in conjunction with the lattice Boltzmann method (Chopard & Droz 1998; Succi 2001) to model the dispersion of nutrients in the external environment by diffusion. The lattice Boltzmann method is especially suitable for developing scalable simulations (using distributed computation) of advection–diffusion/diffusion processes and modelling boundary layers in complex 3D geometries (Kaandorp *et al.* 1996; Koponen *et al.* 1998; Kandhai *et al.* 2002). Simulation of the diffusion process represents the computational bottleneck. Typical run-times of the simulations shown in this paper are 30 h on a parallel machine consisting of 16 processors of 700 MHz each. Details on the equations and parameters used in the lattice Boltzmann simulations and the diffusion model are provided in Appendix A.

### (d) *The accretive growth model*

For our simulations we used the polyp oriented accretive growth model (Merks *et al.* 2004), which derives from differential accretive growth models (Kaandorp & Kübler 2001; Kaandorp & Sloot 2001; Merks *et al.* 2003). The growth process is modelled as a surface-normal deposition process, where new material is deposited along the normal vectors that are constructed on the surface of the previous growth stage (figure 2). X-ray studies demonstrated that the coral polyp tends to be set normal with respect to the previous growth layers (Darke & Barnes 1993; Le Tissier *et al.* 1994). The

Table 1. Description of the parameters used in equations (2.1) and (2.2) for the calculation of the *P*/*R* ratio.

| parameter | description |
|---|---|
| $M_{\text{offset}}$ | metabolic offset from kinetic line |
| $\delta^{13}C_{\text{orig}}$ | measured $\delta^{13}C$ of same skeletal sample as $\delta^{18}O_{\text{orig}}$ |
| $\delta^{13}O_{\text{orig}}$ | measured $\delta^{18}O$ of same skeletal sample as $\delta^{13}C_{\text{orig}}$ |
| $a$ | slope of relation of $\delta^{13}C$ to $\delta^{18}O$ for kinetic isotope fractionation. We used a slope of three which is a rather conservative estimate for establishing *P*/*R* ratios. |
| $\delta^{18}O_{\text{eq}}$ | average $\delta^{18}O$ value for $\delta^{18}O$ of aragonite in equilibrium with sea water, with an average of $\delta^{18}O_{\text{eq}}$ of $0.32 \pm 0.04$ s.e. |
| $\delta^{13}C_{\text{eq}}$ | average $\delta^{13}C$ value for aragonite in equilibrium with sea water, with $\delta^{13}C_{\text{eq}} = \delta^{13}C_{\text{DIC}} + 2.7$ (Heikoop *et al.* 2000). The average $\delta^{13}C_{\text{DIC}}$ was $1.32 \pm 0.02$ s.e. and we thus used a $\delta^{13}C_{\text{eq}}$ of 4.0 |
| $r$ | offset of $\delta^{13}C$ from kinetic line as a result of coral respiration, which is estimated to be $-1.5$ (McConnaughey *et al.* 1997; Heikoop *et al.* 2000) |
| $\delta^{13}C_z/\delta^{13}C_p$ | $\delta^{13}C$ of zooxanthellae/$\delta^{13}C$ of animal polyp from paired samples with an average value of $0.989 \pm 0.003$ |



polyp moves outward with the (living) periphery and leaves a growth trajectory which can be reconstructed by connecting the positions of the centre of a corallite in the successive growth layers. For the simulation model it is therefore assumed that the living tissue deposits new layers of material (aragonite, in the real coral) on top of the previous layers, which remain unchanged. The polyp is carried upwards, vacating the lower skeletal regions. In the real coral, the vacated skeletal regions are separated from the living polyp by dissepiments. This mode of deposition represents an additive-growth pattern of the individual polyps.

In the model, the growth layers are represented by layers of triangles. A small detail of the model is shown in figure 3, where a new layer of triangles (layer $i+1$ with vertices $V_{i+1}$) is constructed on top of the previous layer (layer $i$ with vertices $V_i$). We based the simulation model on the hypothesis that DIC used by photosynthesis is the main limiting factor in the calcification process, and growth is limited by the local amount of nutrient available to the simulated polyp. Light was not considered to be limiting for photosynthesis or coral growth. We assume that inorganic carbon in the immediate environment is exclusively distributed by diffusion. The nutrient distribution was simulated using the diffusion model described above (see Appendix A for details). The diffusion model was coupled to the accretive-growth model, by mapping the geometric representation (the layers of triangles) onto a lattice of $200^3$ nodes. The lattice representation was used for computing the gradients around the simulated growth form. In the diffusion simulations it was assumed that the vertices shown in figure 3 represent the anchor points of the polyps to the skeleton, from which the simulated polyps project along the normal vector. Thus the nutrients are absorbed at a small distance from the simulated coral surface, representing the height of the coral polyps, while the source nodes are located at a certain distance from the object. After the gradients have been computed, the normalized flux of nutrients $c_i$ into the polyp can be calculated. The linear extension rate of the simulated skeleton is driven by the amount of absorbed simulated nutrients. The thickness of a new layer $l_{i+1}$, the distance between two successive vertices $V_i$ and $V_{i+1}$, is computed by using the growth function

$$l_{i+1} = \vec{n}_i c_i s, \tag{2.3}$$

where $\vec{n}_i$ is the average normal vector in vertex $V_i$, $c_i$ is the amount of absorbed simulated nutrients in vertex $V_i$, and $s$ is the maximal thickness of the growth layer. In this growth function we assume a linear relationship between the local amount of deposited material and the local amount of absorbed nutrient from the environment.

In the simulations, the polyps interact locally through the simulated fluid and are closely packed on a growth layer. The distance between the simulated polyp varies around a certain (species-specific) mean size of the polyp. Simulated polyps that become too large split up into new ones, while small ones are deleted. In the figure some triangles in the previous layer $i$ have split up into smaller ones during the construction in layer $i+1$. For further details about the splitting up and deletion of triangles, we refer to aprevious paper on the accretive growth model (Merks *et al.* 2003). After each growth step, where a new layer of triangles is constructed on top of the previous one, we again compute the gradients. We applied 80 growth steps for the simulations in this paper. In the simulated objects shown in this paper we have taken two representative objects of the polyp oriented model; a complete description of simulated growth forms for various polyp distances can be found in Merks *et al.* (2004). The size of the simulated growth form and the number of steps are limited by the dimensions of the simulation box ($200^3$ nodes). The simulation is initialized with a small spherical triangulated object.

The simulated and actual morphologies were quantitatively compared by computing the compactness, $C$, of the objects (Merks *et al.* 2003). $C$ is defined as the ratio

$$C = \frac{V_{\text{object}}}{V_{\text{hull}}} \tag{2.4}$$

of the volume of the object ($V_{\text{object}}$) and the volume of its convex hull ($V_{\text{hull}}$).

## 3. RESULTS

We calculated *P*/*R* ratios of $3.74 \pm 0.11$ ($\pm$ s.e.) and $2.54 \pm 0.08$ for the *M. mirabilis* colonies shown in figure 1*a*,*b*, respectively. This shows that one of our main assumptions in the simulation model, that the metabolism in *M. mirabilis* is mainly supported by photosynthesis, is correct.

Figure 1*a*,*b* shows the reconstructed surfaces of the *M. mirabilis* colonies. $C$ was computed using equation (2.4) for both colonies. For the upward-growing morphology in figure 1*a*, $C$ equals 0.29, whereas in the hemispherical morphology in figure 1*b*, $C$ equals 0.41.

In figure 1*c*,*d* we show examples of simulated morphologies. In figure 1*c* the source of nutrients is located at the top plane and it is assumed that both the simulated polyps and the ground plane absorb nutrients. An absorbing ground plane represents a hard substrate encrusted with absorbing sessile organisms. The hemispherical shape in figure 1*d* is generated by assuming that only the simulated polyps

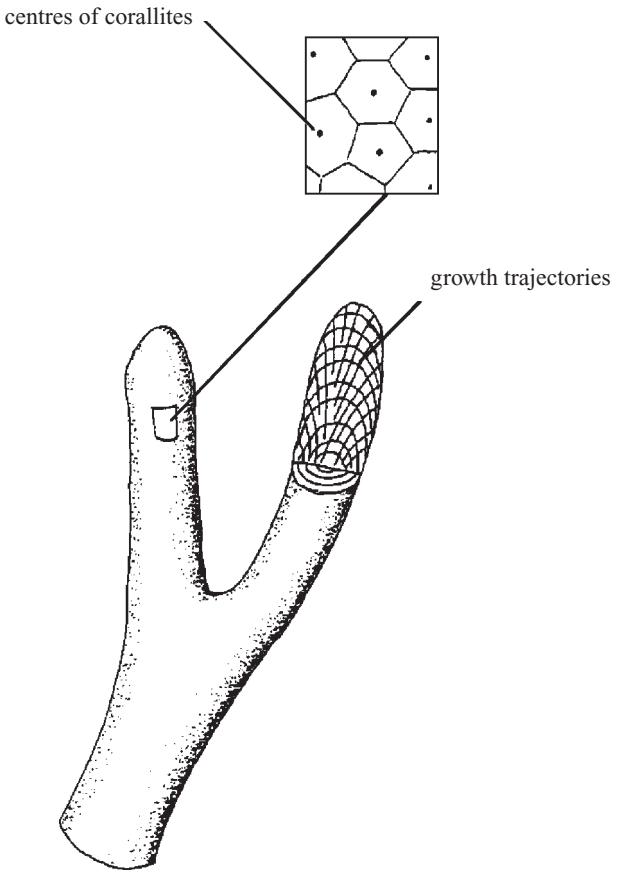


Figure 2. Diagram of the accretive-growth process. Part of the surface is enlarged (see inset), showing the polygons tessellating the surface and the position of the corallites. Part of one branch is removed to show the growth layers and the trajectories of the corallites.

absorb nutrients. $C$ equals 0.30 in the upward-growing morphology shown in figure 1*c* and is 0.24 in the hemispherical morphology (figure 1*d*). A complete description of the simulated growth forms for various polyp distances, boundary conditions, and alternative growth functions is given in Merks *et al.* (2004).

## 4. DISCUSSION

The only species-specific information included in our model is the distance between the polyps and the height of a polyp. Our main discovery is that with the incorporation of simple local rules, controlling the size of individual simulated polyps in the polyp-oriented model (Merks *et al.* 2004), and local gradients it is possible to generate branching morphologies which approximate closely the morphologies of surface renderings of CT scans of *M. mirabilis* shown in figure 1*a*,*b*. In the simulations we obtained *Madracis*-like growth forms *de novo*. Although we did not extensively test the initial conditions in the model, we expect that the model is not very sensitive for the initial conditions in the simulations. We used a spherical object to initialize the growth simulations. After several growth steps, the shape of the initial object hardly influences the shape of the simulated growth form. Another obvious choice for the initial object could, for example, be a sheet of material. A diffusion-limited environment is sufficient to get the correct gradients in the simulated morphogenesis.

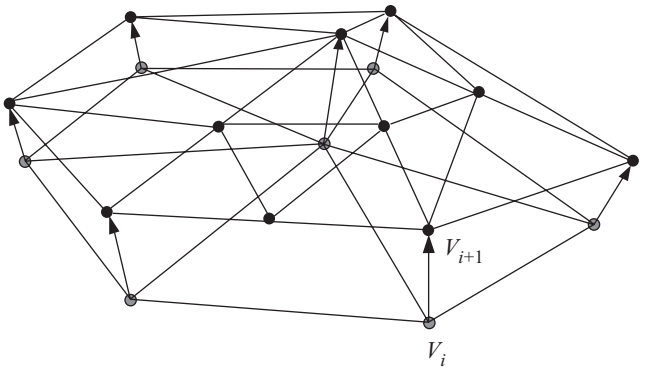


Figure 3. Small detail of the accretive-growth model showing the construction of a new layer (layer $i + 1$) on top of the previous layer (layer $i$). The thickness $l_{i+1}$ of the new layer, the distance between the vertices $V_i$ and $V_{i+1}$, is determined by the growth function in equation (2.3).

When comparing simulated and actual objects in figure 1 we see that the branch spacing, which is quite regular and characteristic in *M. mirabilis* (Sebens *et al.* 1997), is also very regular in both simulated objects. The compactness, $C$ (equation (2.4)), of the simulated objects shown in figure 1 is close to the $C$ values of the actual objects. The results in figure 1*c*,*d* indicate that the model can be used to approximate a branching coral with relatively large closely packed and undifferentiated corallites (e.g. *M. mirabilis*). By slightly modifying the boundary conditions, using an absorbing substrate plane (figure 1*c*) in the upward-growing morphology (figure 1*c*) and a non-absorbing substrate plane in the hemispherical shape (figure 1*d*), it is possible to simulate morphologies of *M. mirabilis* as shown in figure 1*a*,*b*. The upward-growing morphology in *M. mirabilis* is typically found under circumstances when the colony is competing for space and resources with neighbouring colonies, while the hemispherical morphology develops in isolated colonies. The competition effect was represented in the simulation by an absorbing substrate plane.

Intricately branched corals appear to be more susceptible to mortality than massive corals when bleaching occurs during periods of high sea-surface temperatures (Davies *et al.* 1997; Nakamura & Van Woesik 2001; Kaandorp *et al.* 2003; Nakamura *et al.* 2003). One hypothesis is that in intricately branched corals mass transfer through the boundary layer is strongly diffusion-dominated and can disperse fewer of the metabolic by-products that arise during warmer periods (Nakamura & Van Woesik 2001; Nakamura *et al.* 2003). Our results confirm the central role of diffusion-dominated boundary layers, and demonstrate the influence of (external) driving factors in coral functioning and coral growth. Although we have limited our model exclusively to the diffusion-dominated regime, it can be expected that advection still plays an important role in the formation of gradients and boundary layers. For this reason we think it is important to use an advection–diffusion model in combination with a morphogenetic model of the coral. Our results indicate that nutrient gradients may play a major role in the morphogenesis of branching marine sessile organisms with an accretive growth process in general. A similar model can be applied in other scleractinian corals and sponges (Abraham 2001; Kaandorp & Kübler

2001) with a nutrient-limited accretive growth process. In several other cases, for example in the sceleractinian coral *Montastrea annularis* (Graus & Macintyre 1982), the local available light intensity is the major parameter controlling accretive growth. Furthermore it may be hypothesized that in some sessile organisms with accretive growth, the final shape of the organism is controlled by a mixture of parameters (nutrient gradients, local light intensity and hydrodynamics). For a better understanding of growth and form in a morphological highly diverse coral genus like *Acropora* or the diversity within the *Madracis* genus, the influence of genetic factors (Van Oppen *et al.* 2001) and zooxanthellae (Little *et al.* 2004) have to be included in a more detailed morphogenetic model and be compared with actual genetic and morphological data.

We thank L. E. H. Lampmann for his help and advice in obtaining CT scans of the corals; R. G. Belleman and A. Wiegersma for their help with the visualization; A. G. Hoekstra for his advice during the development of the simulations; M. Segl for stable isotope analyses of skeleton and seawater; and S. Schouten for providing the facilities to analyse tissue stable-isotopes. This project was initiated during the 'modelling growth and form of marine sessile organisms' workshop in 1999, funded by the National Science Foundation at the National Center for Ecological Analysis and Synthesis in Santa Barbara, CA.

## APPENDIX A: THE LATTICE BOLTZMANN AND MOMENT PROPAGATION METHOD

The general form of the lattice Boltzmann equation is

$$f_i(x+\Delta t\vec{c}_i,t+\Delta t) = f_i(x,t) + \Omega_i, \tag{A 1}$$

where $f_i$ is the concentration of particles that travels with velocity $\vec{c}_i$. With the discrete velocity, $\vec{c}_i$, the particle distributions travel to the next lattice node in one time step, $\Delta t$. The *collision operator*, $\Omega_i$, differs for the many lattice Boltzmann methods. In the lattice Boltzmann Bhatnagher–Gross–Krook method (Qian *et al.* 1992) that we use, the particle distribution after propagation is relaxed towards the equilibrium distribution $f_i^{\mathrm{eq}}(x,t)$ as

$$\Omega_i = \frac{1}{\tau}\left(f_i(x,t) - f_i^{\mathrm{eq}}(x,t)\right). \tag{A 2}$$

The relaxation $\tau$ parameter determines the kinematic viscosity, $\upsilon$, of the simulated fluid, according to,

$$\upsilon = (2\tau - 1)/6, \tag{A 3}$$

which was set to $\upsilon = 1/6$ for the simulations shown in this paper.

The equilibrium distribution $f_i^{\mathrm{eq}}(x,t)$ is a function of the local density, $\rho$, and the local velocity, $\vec{u}$. These are the first-and second-order moments of the particle distribution given by

$$\rho(x,t) = \sum_i f_i(x,t), \tag{A 4}$$

and

$$\vec{u}(x,t) = \frac{\sum_i f_i(x,t)\,\vec{c}_i}{\rho(x,t)}. \tag{A 5}$$

The equilibrium density $f_i{}^{\mathrm{eq}}(\rho,\vec{u})$ is calculated from

$$f_i{}^{\mathrm{eq}}(\rho,\vec{u}) = t_p\rho\left(1 + \frac{\vec{c}_i\cdot\vec{u}}{c_{\mathrm{s}}^2} + \frac{(\vec{c}_i\cdot\vec{u})^2}{2c_{\mathrm{s}}^4} - \frac{\vec{u}\cdot\vec{u}}{2c_{\mathrm{s}}^2}\right), \tag{A 6}$$

in which $c_{\mathrm{s}}$ is the speed of sound, the index $p = \vec{c}_i\cdot\vec{c}_i$ and $t_p$ is the corresponding equilibrium density for $\vec{u} = 0$. For the 3D, 19 velocity lattice ($D_3Q_{19}$) that we have used in our simulations, $t_0 = 1/3$ (rest particle), $t_1 = 1/18$ (particles streaming to the face-connected neighbours) and $t_2 = 1/36$ (particles streaming to the edge-connected neighbours).

As soon as a steady flow pattern has been obtained with the lattice Boltzmann method, the advection and diffusion of nutrients through the fluid is simulated using the moment propagation method (Lowe & Frenkel 1995; Merks *et al.* 2002). The moment propagation method solves the advection–diffusion equation to second order (Warren 1997). A scalar quantity, $P$, is distributed over the neighbouring lattice nodes, according to the probability, $f_i/\rho$, that a fluid particle moves with velocity, $\vec{c}_i$, after collision,

$$P(x,t+1) = \sum_i \left[\frac{(f_i - \Delta f_i^{\mathrm{eq}}(\vec{u}=0,\rho))p}{\rho}\right]_{x-\vec{c}_i,t} + \Delta P(x,t), \tag{A 7}$$

where the whole quantity inside [...] is evaluated at $(x-\vec{c}_i,t)$, and $\Delta$ is the fraction of resting tracer particles, by which the diffusion coefficient can be set as (Warren 1997; Merks *et al.* 2002)

$$D = \frac{1}{6} - \frac{1}{6}\Delta. \tag{A 8}$$

In this paper $D$ was set to the value 1/6 and $\vec{u}$ was set to 0, the diffusion-limited regime.

## REFERENCES

Abraham, E. R. 2001 The fractal branching of an arborescent sponge. *Mar. Biol.* **138**, 503–510.

Anthony, K. R. N. 1999 Coral suspension feeding on fine particulate matter. *J. Exp. Mar. Biol. Ecol.* **232**, 85–106.

Brener, E., Kassner, K. & Müller-Krumbhaar, H. 1992 Pattern formation in first-order phase transistions. *Int. J. Mod. Phys.* C **3**, 825–851.

Bruno, J. F. & Edmunds, P. J. 1998 Metabolic consequences of phenotypic plasticity in the coral *Madracis mirabilis* (Duchassaing and Michelotti): the effect of morphology and water flow on aggregate respiration. *J. Exp. Mar. Biol. Ecol.* **229**, 187–195.

Chamberlain, J. A. & Graus, R. R. 1977 Water flow and hydromechanical adaptations of branched reef corals. *Bull. Mar. Sci.* **25**, 112–125.

Chopard, B. & Droz, M. 1998 *Cellular automata modeling of physical systems*. Cambridge Univerity Press.

Darke, W. M. & Barnes, D. J. 1993 Growth trajectories of corallites and ages of polyps in massive colonies of reef-building corals of the genus. *Porites*. *Mar. Biol.* **117**, 321–326.

Davies, J. M., Dunne, R. P. & Brown, B. E. 1997 Coral bleaching and elevated sea-water temperature in Milne Bay Province Papua New Guinea 1996. *Mar. Freshwat. Res.* **48**, 513–518.

Graus, R. R. & Macintyre, I. G. 1982 Variation in growth forms of the reef coral *Montastrea annularis* (Ellis and Solander): a quantitative evaluation of growth response to light distribution using computer simulation. *Smitson. Contr. Mar. Sci.* **12**, 441–464.

Heikoop, J. M., Dunn, J. J., Risk, M. J., Schwarcz, H. P., McConnaughey, T. A. & Sandeman, I. M. 2000 Separation of kinetic and metabolic isotopic effects in carbon-13 records preserved in reef coral skeletons. *Geochim. Cosmochim. Acta* **64**, 975–987.

Kaandorp, J. A. 1999 Morphological analysis of growth forms of branching marine sessile organisms along environmental gradients. *Mar. Biol.* **134**, 295–306.

Kaandorp, J. A. & Kübler, J. E. 2001 *The algorithmic beauty of seaweeds, sponges and corals*. Heidelberg, Germany: Springer.

Kaandorp, J. A. & Sloot, P. M. A. 2001 Morphological models of radiate accretive growth and the influence of hydrodynamics. *J. Theor. Biol.* **209**, 257–274.

Kaandorp, J. A., Lowe, C. P., Frenkel, D. & Sloot, P. M. A. 1996 The effect of nutrient diffusion and flow on coral morphology. *Phys. Rev. Lett.* **77**, 2328–2331.

Kaandorp, J. A., Koopman, E. A., Sloot, P. M. A., Bak, R. P. M., Vermeij, M. J. A. & Lampmann, L. E. H. 2003 Simulation and analysis of flow patterns around the scleractinian coral *Madracis mirabilis* (Duchassaing and Michelotti). *Phil. Trans. R. Soc. B* **358**, 1551–1557. (doi:10.1098/rstb.2003.1339)

Kandhai, D., Hlushkou, D., Hoekstra, A. G., Sloot, P. M. A., Van As, H. & Tallarek, U. 2002 Influence of stagnant zones on transient and asymptotic dispersion in macroscopically homogeneous porous media. *Phys. Rev. Lett.* **88**, 23 4501–23 4504.

Koponen, A., Kandhai, D., Hellen, E., Alava, M., Hoekstra, A., Kataja, M., Niskanen, K., Sloot, P. M. A. & Timmonen, J. 1998 Permeability of three-dimensional random fiber webs. *Phys. Rev. Lett.* **80**, 716–719.

Le Tissier, M. D' A. A., Clayton, B., Brown, B. E. & Spencer Davies, P. 1994 Skeletal correlates of coral density banding and an evaluation of radiography as used in scelerochronology. *Mar. Ecol. Prog. Ser.* **110**, 29–44.

Lesser, M. P., Weis, V. M., Patterson, M. R. & Jokiel, P. L. 1994 Effects of morphology and water motion on carbon delivery and productivity in the reef coral, *Pocillopora damicornis* (Linnaeus): diffusion barriers, inorganic carbon limitation, and biochemical plasticity. *J. Exp. Mar. Biol. Ecol.* **178**, 153–179.

Little, A. F., Van Oppen, M. J. H. & Willis, B. L. 2004 Flexibility in algal endosymbioses shapes growth in reef corals. *Science* **304**, 1492–1494.

Lorensen, W. E. & Cline, H. E. 1987 Marching cubes: a high resolution 3D surface construction algorithm. *ACM Comput. Graphics* **21**, 163–169.

Lowe, C. P. & Frenkel, D. 1995 The super long-time decay of velocity fluctuations in a two-dimensional fluid. *Physica* A **220**, 251–260.

McConnaughey, T. A., Burdett, J., Whelan, J. F. & Paul, C. K. 1997 Carbon isotopes in biological carbonates: respiration and photosynthesis. *Geochim. Cosmochim. Acta* **61**, 611–622.

Maier, C., Pätzold, J. & Bak, R. P. M. 2003 The skeletal isotopic composition as an indicator of ecological plasticity in the coral genus *Madracis*. *Coral Reefs* **22**, 370–380.

Marubini, F. & Thake, B. 1999 Bicarbonate addition promotes coral growth. *Limnol. Oceanogr.* **44**, 716–720.

Marubini, F., Ferrier-Pages, C. & Cuif, J. 2002 Suppression of skeletal growth in scleractinian corals by decreasing ambient carbonate-ion concentration: a cross-family comparison. *Proc. R. Soc. B* **270**, 179–184. (doi:10.1098/rspb.2002.2212)

Merks, R. M. H., Hoekstra, A. G. & Sloot, P. M. A. 2002 The moment propagation method for advection-diffusion in the lattice Boltzmann method: validation and Peclet number limits. *J. Comput. Phys.* **183**, 563–576.

Merks, R. M. H., Hoekstra, A. G., Kaandorp, J. A. & Sloot, P. M. A. 2003 Models of coral growth: spontaneous branching, compactification and the Laplacian growth assumption. *J. Theor. Biol.* **224**, 153–166.

Merks, R. M. H., Hoekstra, A. G., Kaandorp, J. A. & Sloot, P. M. A. 2004 Polyp oriented modelling of coral growth. *J. Theor. Biol.* **228**, 559–576.

Muko, S., Kawasaki, K., Sakai, K., Takasu, F. & Shigesada, N. 2000 Morphological plasticity in the coral *Porites sillimaniani* and its adaptive significance. *Bull. Mar. Sci.* **66**, 225–239.

Nakamura, T. & Van Woesik, R. 2001 Water-flow rates and passive diffusion partially explain differential survival of corals during the 1998 bleaching event. *Mar. Ecol. Prog. Ser.* **212**, 301–304.

Nakamura, T., Yamasaki, H. & Van Woesik, R. 2003 Water flow facilitates recovery from bleaching in the coral *Stylophora pistillata*. *Mar. Ecol. Prog. Ser.* **256**, 287–291.

Qian, Y. H., D'Humieres, D. & Lallemand, P. 1992 Lattice BGK models for the Navier-Stokes equation. *Euorophys Lett.* **17**, 479–484.

Schroeder, W., Martin, K. & Lorensen, B. 1997 *The visualization toolkit: an object-oriented approach to 3D graphics*, 2nd edn. Englewood Cliffs, NJ: Prentice-Hall.

Sebens, K. P., Witting, J. & Helmuth, B. 1997 Effects of water flow and branch spacing on particle capture by the reef coral *Madracis mirabilis* (Duchassaing and Michelotti). *J. Exp. Mar. Biol. Ecol.* **211**, 1–28.

Sorokin, Y. I. 1993 *Coral reef ecology*. Heidelberg, Germany: Springer.

Succi, S. 2001 *The lattice Boltzmann equation: for fluid dynamics and beyond*. Oxford University Press.

Van Oppen, M. J. H., McDonald, B. J., Willis, B. L. & Miller, D. J. 2001 The evolutionary history of the coral genus *Acropora* (Scleractinia, Cnidaria) based on mitochondrial and a nuclear marker: reticulation, incomplete lineage sorting, or morphological convergence? *Mol. Biol. Evol.* **18**, 1315–1329.

Veron, J. E. N. & Pichon, M. 1976 *Scleractinia of Eastern Australia. Part V. Family Acroporidae*. Canberra, Australia: Australian Government Publishing Service.

Warren, P. B. 1997 Electroviscous transport problems via lattice-Boltzmann. *Int. J. Mod. Phys.* C **8**, 889–898.

As this paper exceeds the maximum length normally permitted, the authors have agreed to contribute to production costs.

Visit www.journals.royalsoc.ac.uk and navigate through to this article in *Proceedings*: Biological Sciences to see the accompanying electronic appendix.